Science of the Total Environment 635 (2018) 1467–1476

Contents lists available at ScienceDirect

Science of the Total Environment

journal homepage: www.elsevier.com/locate/scitotenv

Impact of urbanization-related land use land cover changes and urban morphology changes on the urban heat island phenomenon

Xuefan Zhou, Hong Chen *

School of Architecture and Urban Planning, Huazhong University of Science and Technology, China

HIGHLIGHTS

- When the lake area decreased by 130 km^2 in the built-up area of Wuhan, UHI intensity increased by 0.2 °C–0.4 °C.
- When the lake area decreased by 130 km^2, the critical value of wind speed needed to mitigate the UHI doubled at 04:00.
- Air temperature differences between these two development patterns can reach 1 °C and that at 12:00 and 17:00, respectively.
- The critical values of wind speed in the high-density case were 1.5 and 2 times higher than those of the high-rise case.
- The T2 in the high-density case was 0.5 ºC higher, however, wind speed of high-rise case was 70% of high-density case.

GRAPHICAL ABSTRACT

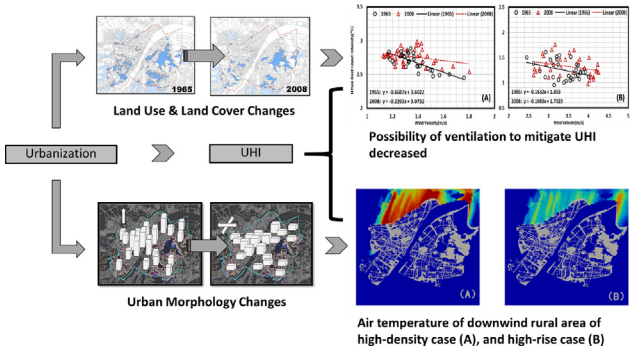

ARTICLE INFO

Article history:
Received 8 February 2018
Received in revised form 21 March 2018
Accepted 6 April 2018
Available online 25 April 2018

Editor: Scott Sheridan

Keywords:
UHI
LUCC
Development patterns
Urban morphology
Compact city

ABSTRACT

Urban growth and development caused by urbanization influence the urban heat island (UHI) phenomenon. With the rapid development of urbanization, China's major cities are facing more serious climate change problems, especially the UHI phenomenon. Proper planning and urban design of compact cities may improve the ventilation of street canyons and change the heat balance in the urban canopy and thus mitigate the UHI phenomenon. The aim of this study is to evaluate and discuss the mitigation of UHI with different types of land-use and land-cover (LUCC), as well as different development patterns for compact cities. To this end, we applied the weather research and forecasting model (WRF) with urban canopy model (WRF/UCM) in this study. To evaluate the impact of LUCC changes on the UHI, we set 2 cases based on land use and land cover statistical data from 1965 and 2008 of Wuhan. Also, to evaluate the impact of urban morphology changes on the UHI, we designed 2 hypothetical cases based on 2 different urban developing patterns, one is high rise case and another is high density case, to simulate the impact of urban morphology on the UHI. As for the results of this study, with different LUCC of 1965 and 2008, UHI intensity of Wuhan increased by 0.2 °C–0.4 °C in average. Moreover, the critical wind speed which can mitigate UHI of case 1965 is much lower than case 2008. With different urban morphology, the high-rise case may lead to lower UHI intensity at the pedestrian level due to the shading effects of high-rise buildings. However, the critical value of wind speed in the high-rise case was almost 1.5–2 times greater than that of the high-density case, which illustrates the reduced possibility of mitigating the UHI phenomenon for high-rise buildings in Wuhan City.

* Corresponding author at: School of Architecture and Urban Planning, Huazhong University of Science and Technology, Luoyu Road 1037, Wuhan, Hubei, 430074, China.
E-mail addresses: xuefanzhou@hust.edu.cn, (X. Zhou), chhwh@hust.edu.cn. (H. Chen).

https://doi.org/10.1016/j.scitotenv.2018.04.091
0048-9697/

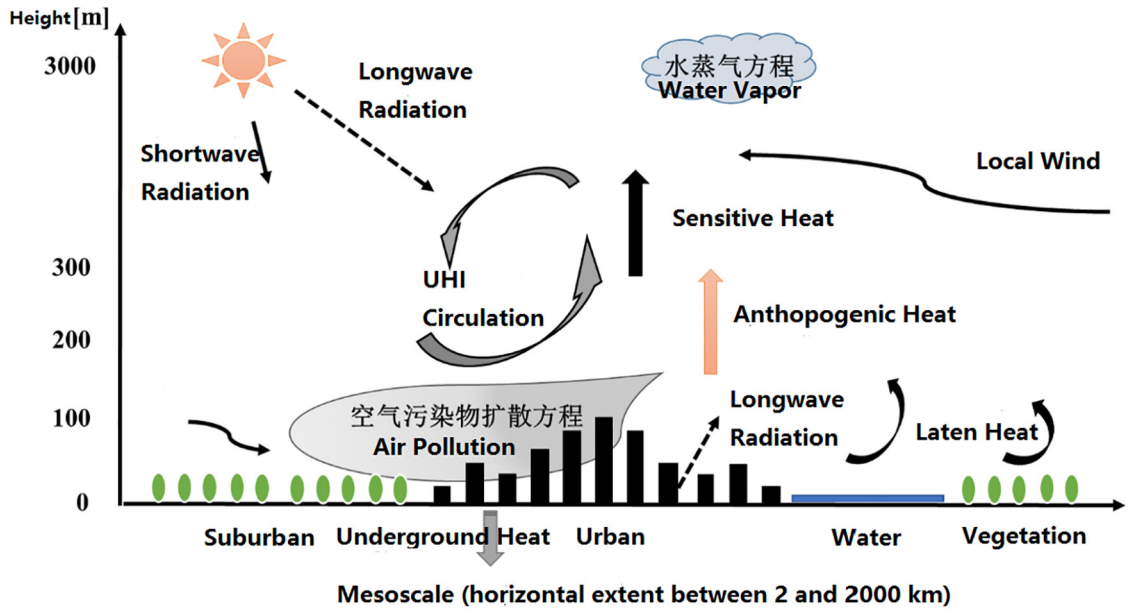

Fig. 1. Meso-scale simulations in WRF (SLAB, WRF/UCM, and WRF-Chem).

1. Introduction

According to the annual report of the NBS (National Bureau of Statistics) of China, by the end of 2014, 54.7% of the total population lived in urban areas, and it is predicted that by 2020, the urbanization rate will reach 60% (Niu, 2013). Urbanization refers to the population shift from rural to urban areas, which is a world-wide phenomenon that is not only taking place in China. It is predicted that by 2050, approximately 64% of the developing world and 86% of the developed world will be urbanized (The Economist, 2012). Rapid urbanization may sometimes cause urban sprawl, which may result in the conversion of farmland, wetland or lakes into urban areas. And also, Rapid urbanization may densify built-up zones and increase building density, compactness, plot ratio, and average building height, as well as changing the urban morphology. It has been observed that climate change caused by urbanization may even lead, in the case of Malawi, to reverse (i.e., urban to rural) migration (Suckall et al., 2015). Besides climate and environment changes, rapid urbanization is assumed to a major factor causing the urban heat island (UHI) phenomenon, which refers to a city or metropolitan area's being significantly warmer than its surrounding rural areas, due to human activities.

The urban heat island (UHI) phenomenon was first discovered by Luke Howard in London in 1818, the phenomenon has subsequently been recognized to exist in many countries and regions worldwide. And it is one of the most serious urban climate and environmental problems. Compared to rural areas, the urban underlying surface usually has high heat capacity and thermal conductivity and is mostly waterproof material. Moreover, building surfaces extend the area of the urban underlying surface, which causes multiple reflections and absorption. Therefore, these properties increase the quantity of heat flux absorbed and stored in urban areas. Even worse, there are many high buildings in the city, which increases the roughness of the urban area, thus reducing urban ventilation. Due to the special characteristics and morphology of urban areas, heat absorption, storage and heat convection increase, causing a large quantity of heat to remain and accumulate. Moreover, the anthropogenic heat form human activities also adds to this accumulated heat. Therefore, compared to rural areas, there is a greater tendency for urban areas to experience higher outdoor air temperature levels (up to 12 K higher) (Gaur et al., 2018).

How the urban heat island phenomenon can be effectively relieved has always been a key question. Recently, as cities expand and develop increasingly rapidly, many researchers have begun to study the relationship between urban morphology and the urban heat island phenomenon (Dhar and Khirfan, 2017; Li et al., 2017; Liu et al., 2018; Sharma and Joshi, 2016). Lin et al. (2017) have noticed that such factors as building height, building density, road width and orientation can affect the heat balance in urban canyons. With increasing urbanization, the UHI phenomenon is becoming more of a concern, with urban heat island intensities continuing to increase, especially, in many megacities (dos Santos et al., 2017; Yao et al., 2017). Due to the negative effects of UHIs in hot periods, in summer, the urban thermal environment is increasingly unendurable, with residents relying on air conditioners to a greater degree than in the past. This reliance, in turn, greatly increases the quantity of anthropogenic heat release, forming a vicious circle worsening the negative effects.

Therefore, well-planned cities can greatly improve the urban thermal environment and relieve the urban heat island phenomenon (Lin et al., 2017). To prevent urban overdevelopment from destroying the urban climate and environment, cities should be planned carefully before they are fully developed, and this planning should be based on quantitative guidance.

The major objective of this study is to quantitatively evaluate the impact of changes in urban forms under rapid urbanization on the urban heat island phenomenon. Based on a case study in Wuhan, the capital city of Hubei province in China, we discuss the land use and land cover changes during its urbanization. This approach is employed to estimate the changes in urban climate and environment which have accompanied its urbanization. Additionally, we will also simulate the impact of the built-up area of the city's becoming progressively more compact. To provide quantitative urban planning guidance to improve

Table 1
Schemes selected in WRF.

Boundary layer physics	Mellor-Yamada Janjic (ETA) TKE scheme
Surface layer physics	Monin-Obukhov (Janjic Eta) scheme
Surface physics	Unified Noah land-surface model
Microphysics	Thompson graupel scheme (2-moment scheme in V3.1)
Longwave radiation physics	RRTM (rapid and accurate radiative transfer)
Shortwave radiation physics	Goddard shortwave scheme

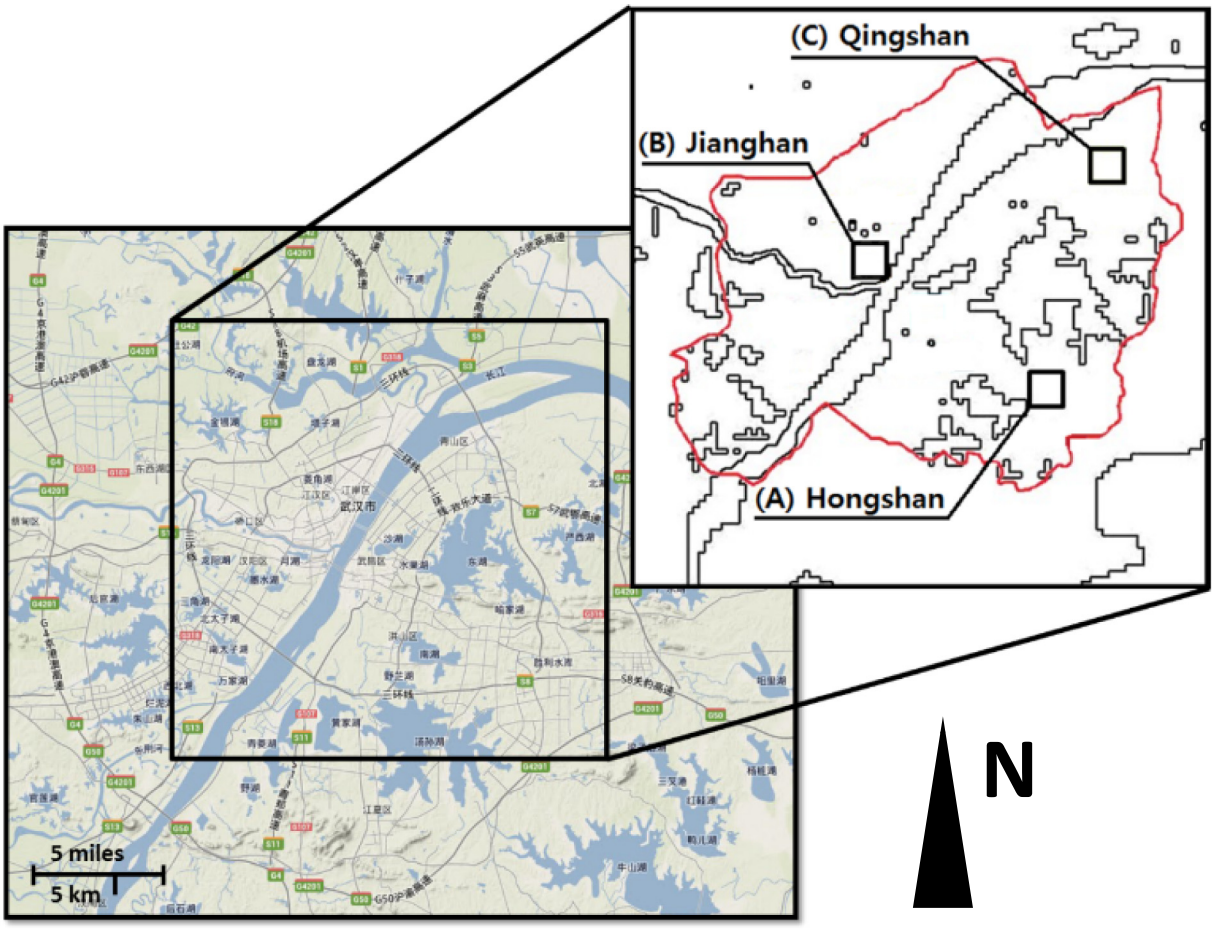

Fig. 2. Map of study area showing sampling blocks within the Hongshan, Jianghan, and Qingshan districts.

the urban thermal environment, consequently, we simulated the impact of developing patterns (high-density or high-building) on the urban climate and environment during the urbanization of Wuhan.

The study includes the following two concrete aspects:

a. From 1965 to 2008, the wetland and lake areas decreased 130.5 km^2 in the built-up area of Wuhan, which is ⅓ of the total water area in Wuhan. We aim to investigate the impact of the LUCC changes during its urbanization using Wuhan as a case study of the urban climate and environment, especially regarding the UHI effect.

b. In addition to land-use and land-cover changes, it has been predicted that the area of land used for urban construction will increase in the built-up area. Therefore, these areas will become more compact due to the population explosion in recent years. By 2020, the total population will reach 11.8 million, while the population of the built-up area will total 5.02 million, and the rate of urbanization may reach 84 %. As a result, by 2020, the total area of land used for urban construction in Wuhan will increase to 1030 km^2, and the area of land used for urban construction in the built-up area of Wuhan will rise to 450 km^2.

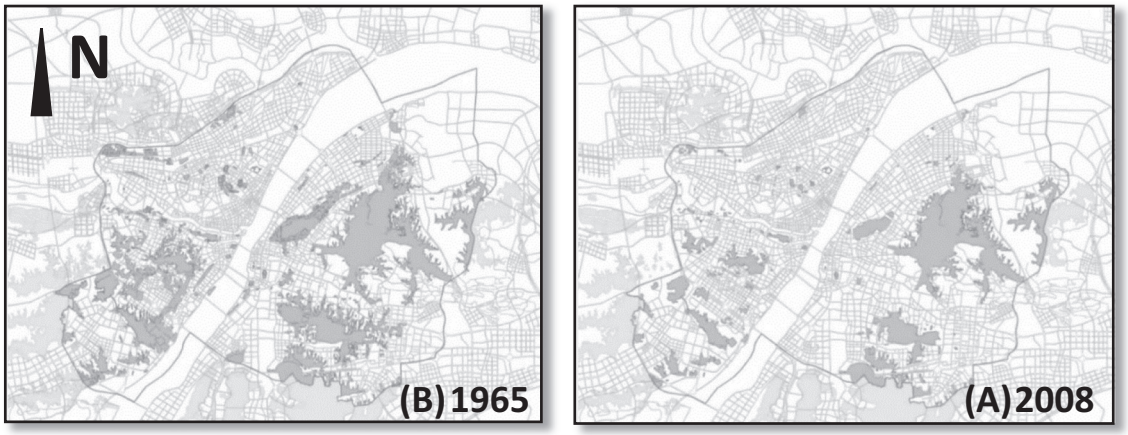

Fig. 3. Map showing lake area (gray block) distribution in 1965 (A), and 2008 (B) in built-up area of Wuhan.

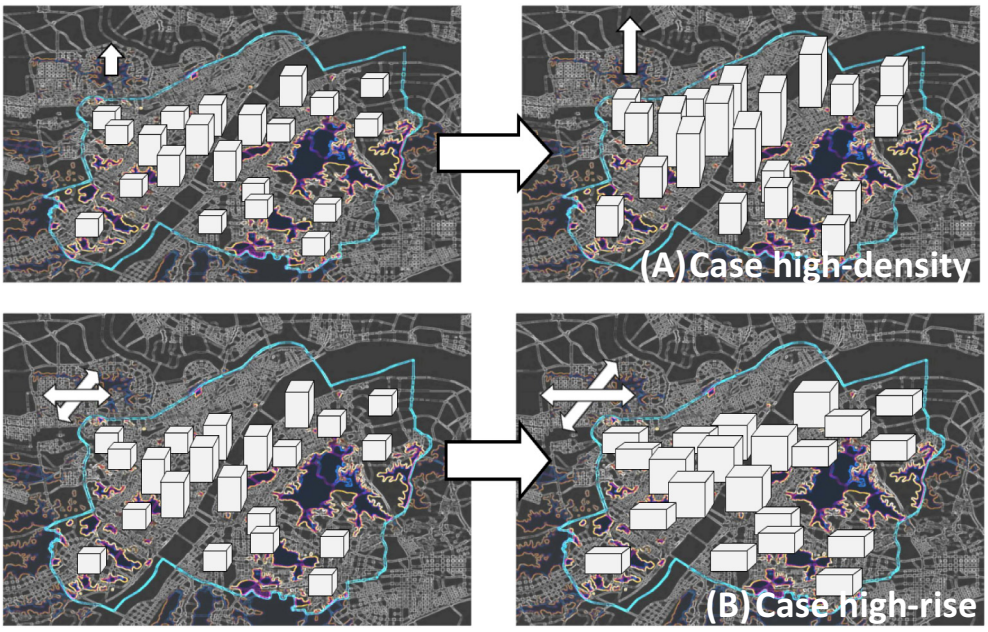

Fig. 4. Concept of the high-density case (A) and high-building case (B).

2. Previous work

As mentioned above, how the urban heat island phenomenon can be effectively relieved has always been a key question. Many solutions from different perspectives and on different scales have been provided. For example, Hsieh C, Aramaki T, and Hanaki K studied the negative effects of exhaust heat from air conditioners on the urban heat island. These researchers observed that properly designing the outdoor part of the air conditioner would greatly reduce the impact on the thermal environment at pedestrian level and thus greatly improve outdoor human thermal comfort (Hsieh et al., 2011). Others believe that urban greenery is one of the most effective solutions, and many countries and regions have added roof and facade greening to their official city planning to relieve the urban heat island (Alcazar et al., 2016; Lin et al., 2018; Yan et al., 2018). Tsunematsu et al. (2016) suggested increasing the rate of building volume in order to enable more green spaces. This method has been implemented in Otemachi, Tokyo. Using thermal infrared techniques, temperature decreases were noticed between the before and after cases (Tsunematsu et al., 2016). Vox et al. (2017) have suggested architecture selecting proper building surface materials and, according to their study results, recommended using high reflection and heat insulation materials to block heat from the building facades and to reduce heat storage in building structures. This strategy can effectively ease the urban heat island intensity during the night.

And on a broader scale, many researchers have noticed the impact of urban morphology on UHI phenomenon. Moreover, the changes in the urban underlying layer is assumed to be the major factor causing the UHI phenomenon. For example, due to LUCC changes, the albedo, thermal conductivity, capacity, and conservation of underlying surfaces are changed (Sato et al., 2008). In the Atlanta metropolitan area, maximum annual land surface temperature differences of 5.7 K were generated by the LUCC changes from evergreen forest to medium-intensity urban land (Fu and Weng, 2016). A significant negative relationship between distance from the center of the city and heat intensity was discovered in Addis Ababa, Ethiopia, indicating the increasing thermal consequences of the rapid urbanization (Feyisa et al., 2016). Due to the LUCC changes, the 2 m air temperature in Putrajaya is increasing at the rate of 1.66 °C per decade, while the prevailing urban heat island intensity (UHII) of the area is approximately 2.1 °C (Morris et al., 2016).

Not only LUCC changes may impact the UHI effect, as nowadays our urban morphology become higher and denser, and due to the multiple reflections between buildings, more short- and long-wave radiation is absorbed in street canyons (Nunez and Oke, 1977). What's more? The windshield of high buildings also decreases the heat loss by convection (Lopes et al., 2011), while the concentration of population due to urbanization increases anthropogenic heat release. As much more heat is stored in the artificial underlying layers during daytime, and more heat is released to warm the atmosphere at night (Fahmy and Sharples, 2009). Therefore, the heat balance of the area is affected, causing a more serious UHI effect.

As we may notice that more and more researchers begin to realize the serious influence of urban morphology on the UHI phenomenon. However, a majority of the studies were just focus on observation of the intensification of UHI phenomenon with rapid urbanization using satellite remote sensing techniques coupled with Geographic Information System (GIS). Due to the limitation of simulation techniques, just a few studies did sensitivity analysis of urban morphology to UHI effect,

Table 2
Case settings (Average values in the built-up area of Wuhan).

Cases	Water Area (m^2)	Building density (%)	Plot ratio	Greenery ratio (%)	Average roof level (m)	Average roof width (m)
Case_1965	518.25	–	–	–	–	–
Case_2008	387.75	–	–	–	–	–
Case_high-density	–	65	5.0	55	30	60
Case_high-rise	–	35	10.0	25	90	30

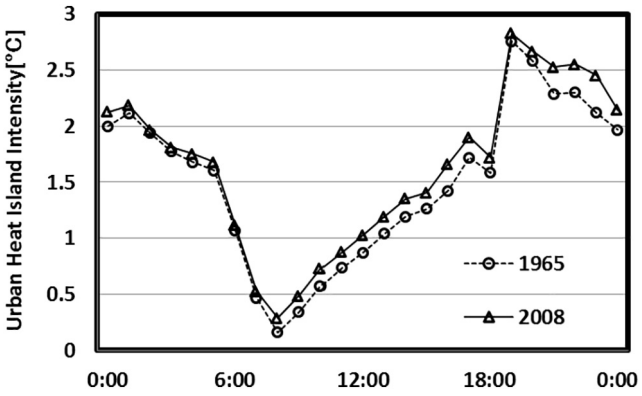

Fig. 5. Total area average diurnal UHI intensity of the built-up area for Case_1965 and Case_2008.

not to mention the prediction of UHI intensity growth trend along with urbanization and the quantitative urban morphology planning strategies on UHI mitigation. Therefore, this study tries to make an attempt to find some quantitative planning strategies with Weather Research and Forecasting Model (WRF).

3. Methodology

To obtain the urban scale simulation in this study, we applied the next-generation mesoscale numerical weather prediction system Mesoscale Meteorological Model (MMM) of the Weather Research and Forecasting Model (WRF). This model was developed by the National Center for Atmospheric Research (NCAR) and National Center for Environmental Prediction (NCEP) and was used in this study to predict the impact of land use and land cover and urban morphology changes on the urban heat island phenomenon. In WRF, there are two running modes to choose from, one is a real case mode for simulating the current situation of real cities, and the other is the ideal case to simulate virtual cities. The WRF model is a fully compressible and non-hydrostatic model (with a run-time hydrostatic option) (Avolio et al., 2017). This model's vertical coordinate is a terrain-following hydrostatic pressure coordinate. The grid staggering is the Arakawa C-grid. The WRF model works for meso-scale phenomena such as sea breezes and mountain valley flows with large area coverage at coarse resolution (Kusaka et al., 2001; Xue et al., 2017). The WRF model predicts wind velocity, wind direction, temperature, water vapor, cloud cover, precipitation, and pressure distribution on different underlying surfaces (Birch et al., 2017). However, anthropogenic effects and urban morphology are not fully considered in the basic WRF model.

Beside the WRF-basic SLAB model, the Urban Canopy Model (UCM) is used for urban climate study and the Chemical Model for studying atmospheric pollutants. As shown in Fig. 1, these two extra models function as plug-in components to strengthen WRF's climate simulating capability. Therefore, the WRF is now capable of simulating the physical and chemical processes of the urban climate and environment, such as the absorption and reflection of long wave and shortwave radiation in buildings (Wai et al., 2017), the vaporization process, vegetation transpiration, the diffusion process of air pollutants, and urban heat island circulation.

In this study, we use the single-layer urban canopy model of WRF, which was originally developed by Chen et al. (2011). As is known, the urban canopy layer is the closest layer to the land surface below the top of the buildings. This layer has the most direct impact on the urban boundary layer and is also one of the most important factors in forming the urban microclimate. The WRF/UCM is able to calculate the following influencing factors: (1) Blocking effect of air-flow on buildings and vegetation; (2) Turbulence effects around buildings and vegetation; (3) Multiple reflections in urban canyons; (4) Anthropogenic heat emissions from buildings and traffic; and (5) Shading effect of vegetation. Therefore, together with UCM, being able to calculate the impact of buildings on the atmosphere and add it to heat balance equations, the WRF can be used to predict the climate and environment of cities.

For more details, the Monin and Obukhov scheme for surface layer physics (Monin and Obukhov, 1954), the Thompson et al. (2004) scheme for microphysics, the Mlawer et al. (1997) scheme for longwave and shortwave radiation physics, and the Noah scheme for a land surface model (LSM) (Chen and Dudhia, 2001) were selected in this study. The above information is summarized and shown in Table 1.

Relative to calculating the resolution and accuracy of WRF/UCM, validation was completed prior to this study, and the results were provided in our recently published paper (Zhou et al., 2016). These results provided confidence in the model as a predictive tool that can be used to estimate the change in local climates and thermal environments. Therefore, validation was not repeated for this study.

4. Study area and setting

4.1. Study area

Wuhan is located at the confluence of the Han and Yangtze Rivers along the middle reaches of the latter. The development of Wuhan has been accelerating, and this city has recently been elevated to the first tier of cities, such as CBN Weekly (2015). Wuhan occupies a land area of 8494.41 km^2, 888 km^2 of which is the built-up area. By 2013, the population of Wuhan had reached 10.22 million, and the area of land used for urban construction in the built-up area had reached 795 km^2. The

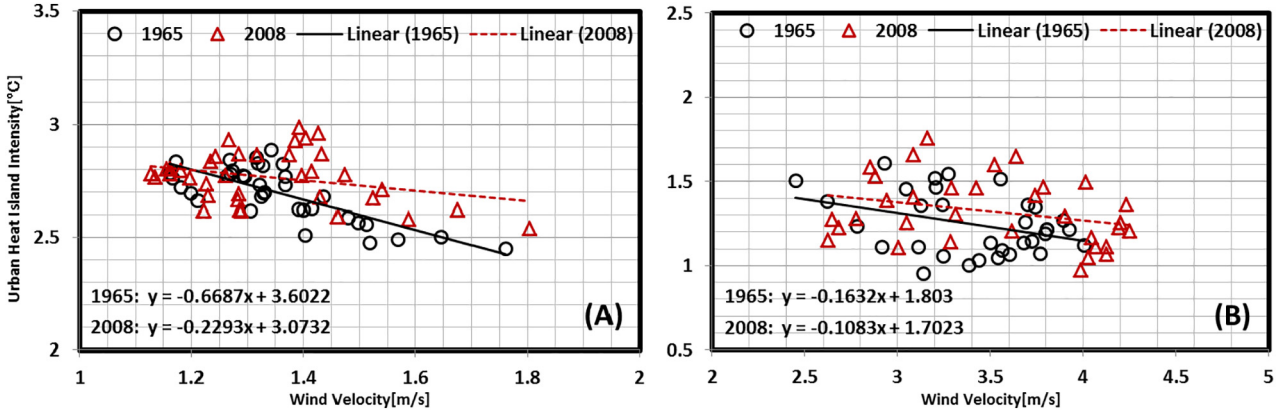

Fig. 6. Scatter plots for UHI intensity and wind speed for Case_1965 and Case_2008 in the Jianghan sampling zone at 04:00 (A), and 12:00 (B).

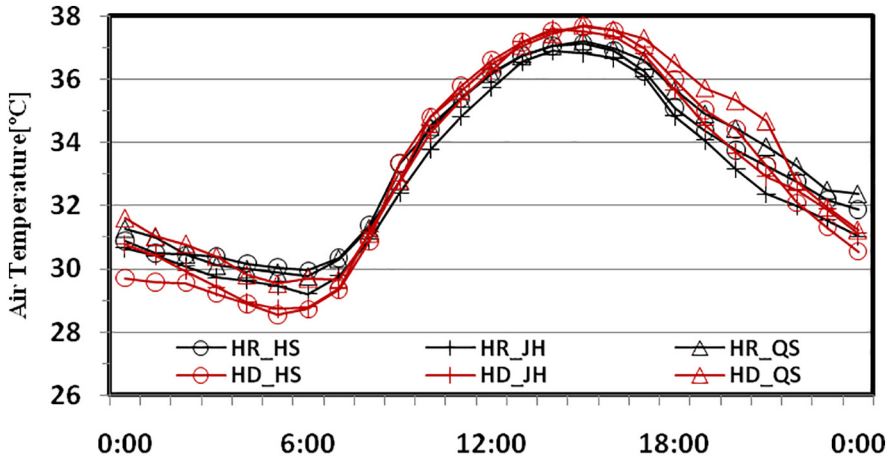

Fig. 7. Plot of diurnal air temperature of Hongshan district (HR_HS), Jianghan district (HR_JH), and Qingshan district (HR_QS) for Case_high-rise; and Hongshan district (HD_HS), Jianghan district (HD_JH), and Qingshan district (HD_QS) for Case_high-density.

population of the built-up area had reached 4.4 million. Wuhan belongs to the humid subtropical climate zone with abundant rainfall and four distinct seasons. The summer period lasts almost 135 days a year, while the spring and autumn periods together total 120 days a year. The prevailing wind directions in summer and winter are southeast and northwest, respectively. In particular, Wuhan has a historical reputation for a harsh local climate. Wuhan is known for its oppressively humid summers, insofar as it is a typical city with hot humid climates (Wu et al., 2014). During its rapid urbanization, Wuhan has undergone a severe urban heat island effect.

As shown in Fig. 2, the study area is at latitude 30.25°N–30.7°N and longitude 114°E–114.55°E, which corresponds to the built-up area of Wuhan. For the simulation study, we set 3 domains and the finest mesh to 500 m. To more closely examine the effects of urban form, we selected three sampling zones from the Hongshan, Jianghan and Qingshan districts. The Hongshan sampling zone is close to a suburban area located upwind of Wuhan and is surrounded by inland lakes. Thus, it was anticipated that water would exert particular effects on this area. The Jianghan sampling zone is located on the north shore of the Yangtze River in the center of Wuhan. Given this zone's proximity to the Yangtze River, this district's ventilation is primarily reliant on winds coming from the river. Jianghan is also one of the largest commercial districts in Wuhan, and its building density and floor area ratio are thus comparatively high. Finally, the Qingshan sampling zone is located on the south shore of the Yangtze River downwind of Wuhan.

4.2. Case settings

For this study, we designed four cases in two groups to quantitatively investigate the impact of urban form. The first group of cases regard land-use and land-cover changes, and the cases are based on the lake area in Wuhan's decrease from 1965 to 2008. The second group

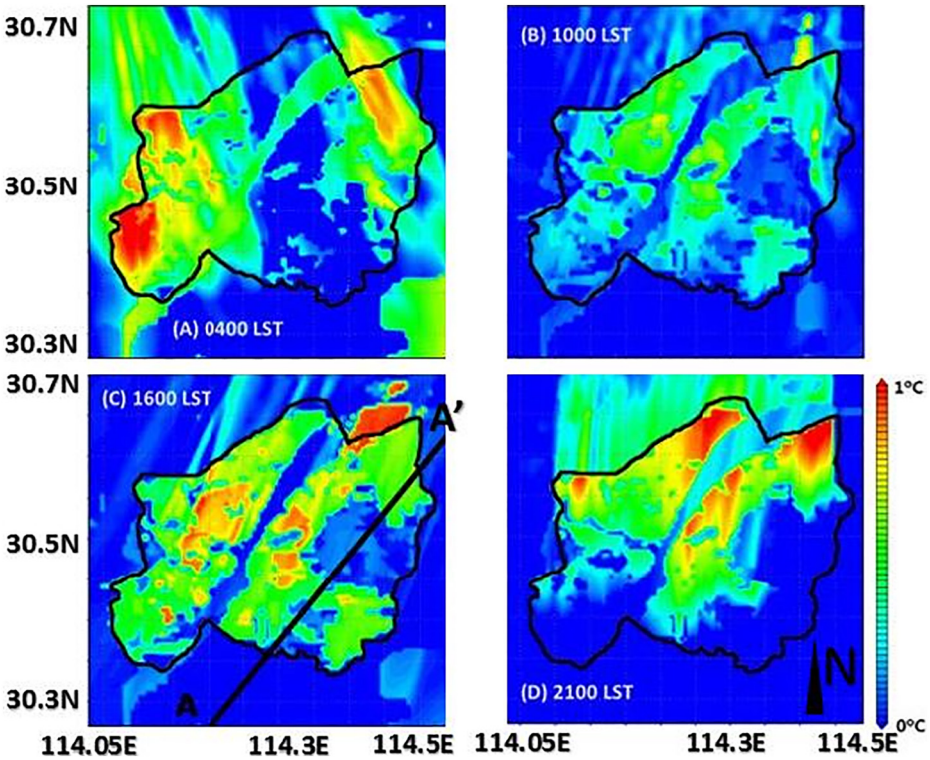

Fig. 8. Map of distribution of air temperature differences between the high-density case and high-rise case of Wuhan ($T2_{HD}$-$T2_{HR}$).

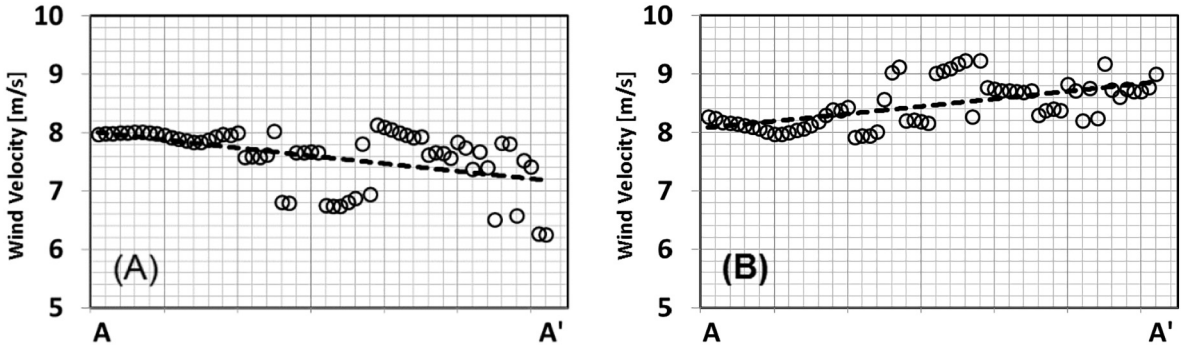

Fig. 9. Scatter plot showing gradient of wind velocity along the sampling line for high-rise case (A), and high-density case (B).

of cases involve the compact development of urban morphology in Wuhan. We designed high-density and high-building cases based on a compact city development pattern for Wuhan based on the 2020 master plan.

As shown in Fig. 3, during the period from 1965 to 2008, the lake area (gray color) of the built-up area of Wuhan has decreased from 518.25 km^2 (Fig. 3A) to 387.75 km^2 (Fig. 3B). The first group of cases of lake area distribution and changes are based on Fig. 2, and we named these 2 cases Case_1965 and Case_2008. The only differences between Case_1965 and Case_2008 consist of the area and distribution of the lakes.

Fig. 4 presents the concept of the high-density case (Fig. 4A) and high-building case (Fig. 4B). We predicted that the area of land used for urban construction in the built-up area will increase to 450 km^2 by 2020. To fulfil the requirements of urban development, with 89 m^2 of living space per person for 5.02 million people in the built-up area, we assumed two compact city development patterns and named them Case_high-density and Case_high-rise. These two cases share the same area of land used for urban construction, and the morphology of urban growth is the only difference between the two cases. The details of the case settings are provided in Table 2.

4.3. Data source

Hourly meteorological data of air temperature, relative humidity, and wind velocity and direction applied in this study is provided by Hubei Meteorological Bureau (http://www.hbqx.gov.cn/index.action). We applied NCEP Final Analysis (GFS-FNS) ds083.2 meteorological dataset for WRF simulation as boundary conditions. The spatial resolution of this data is 1°, with 6-hourly temporal resolution from 1999 to 07-03 to current (http://www2.mmm.ucar.edu/wrf/users/download/free_data.html).

Water area data from 1965 to 2008 applied in this study is supplied by Wuhan Land Resources and Planning Bureau (http://gtghj.wuhan.gov.cn/). Case setting data of Case_high-density and Case_high-rise such as building density, plot ratio, greenery ratio, average roof level, and average roof width are set based on the control index of Wuhan general urban planning for 2020. The final data is calculated and predicted according to the increasing area of land used for urban construction in the built-up area by 2020.

5. Results

5.1. Impact of land-use and land-cover changes on UHI

In the drive to achieve rapid economic growth, land reclamation of lakes in the built-up area of Wuhan has been underway since the last century. According to the record, land-use and land-cover has changed significantly in the built-up area of Wuhan from 1965 to 2008, with the lake area decreasing by 130.5 km^2 in the built-up area, which is approximately ⅓ of the total lake area. To investigate the impact of land-use and land-cover changes on UHI phenomenon, we compared Case_1965 and Case_2008. Fig. 5 presents the total area average diurnal UHI intensity of the built-up area for Case_1965 and Case_2008.

Due to the decrease in lake area, the UHI intensity increased, especially from 20:00 to 24:00, during which UHI intensity grew by 0.3 to 0.4 °C. In contrast, from 8:00 to 18:00, the growth of UHI intensity was approximately 0.2.

The two periods mentioned above are the periods with the most distinct impact of land-use and land-cover changes on the UHI phenomenon. During the period from 20:00 to 24:00, the lake area functions as open space in the city, which can help ventilate the urban area and dissipate gained heat in the urban canopy. In contrast, during the period from 8:00 to 18:00, the lake area functions as the “cold source” for the urban atmosphere because of its high specific heat capacity.

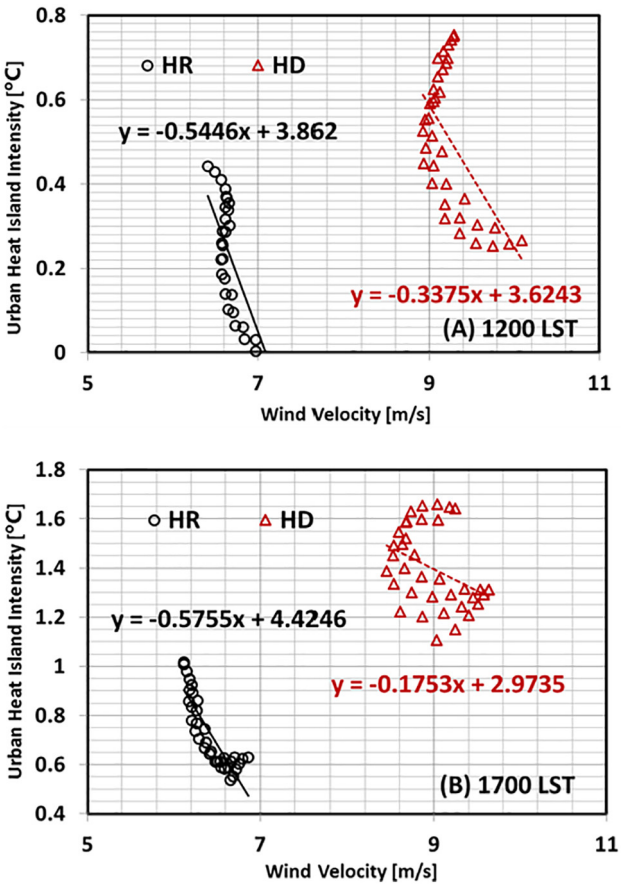

Fig. 10. Scatter plot of UHI intensity and wind speed in Case_high-density and Case_high-rise for Qingshan sampling zone at 04:00 (A), and 12:00 (B).

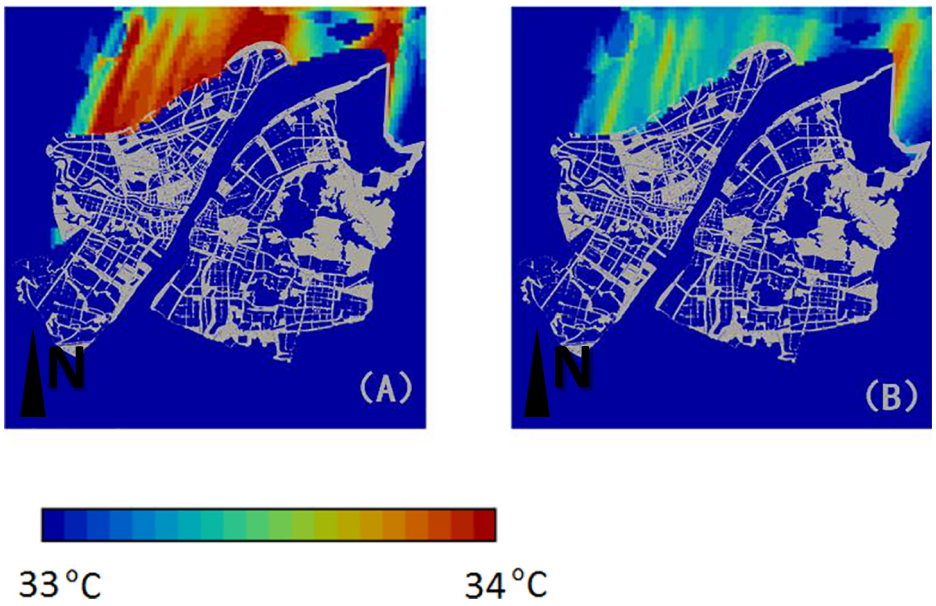

Fig. 11. Map of distribution of air temperature in Case_high-density (A), and Case_high-rise (B) at 20:00.

As discussed above, the decrease in lake area increased the total area average UHI intensity of the built-up area of Wuhan. Moreover, the decrease in lake area also increased the critical values of wind speed that could mitigate the UHI phenomenon. Fig. 6 presents the scatter plot for UHI intensity and wind speed in Jianghan sampling zone. The black circles represent the set of data for Case_1965, while the red triangles represent the set of data for Case_2008. When UHI intensity (y-axis) approaches zero at 04:00, the critical values of wind speed are 5.4 m/s and 13.4 m/s for Case_1965 and Case_2008, respectively. At mid-day (12:00), the critical values of wind speed are 11.1 m/s and 15.7 m/s for Case_1965 and Case_2008, respectively. The above results show that the decrease in lake area may greatly reduce the possibility of mitigating the UHI phenomenon through urban ventilation. Data from the Wuhan weather station show that the average annual wind speed in Wuhan is 2.8 m/s, the maximum annual wind speed is 19.1 m/s, and the highest wind speed is 28 m/s. Therefore, we can assume that because of the lake area in the built-up area of Wuhan, the UHI phenomenon in 1965 was not as serious as in 2008, especially at 04:00. This finding indicates that night-time ventilation cooling was quite effective before the areas of lake vanished. However, with urbanization in recent years, that cooling effect has been gradually reduced.

5.2. Impact of changes in urban morphology on urban climate

Fig. 7 gives the diurnal air temperature of different sampling zones in Case_high-density and Case_high-rise. Fig. 8 provides the distribution of the air temperature difference between the two cases at different times. Generally, for each sampling zone, the midday air temperature in Case_high-density is 1 °C higher than that in Case_high-rise. This finding is observed because, firstly, at midday, the solar elevation angle is notably high such that the shading effect of high buildings is more significant in Case_high-rise, and second, the green area in Case_high-

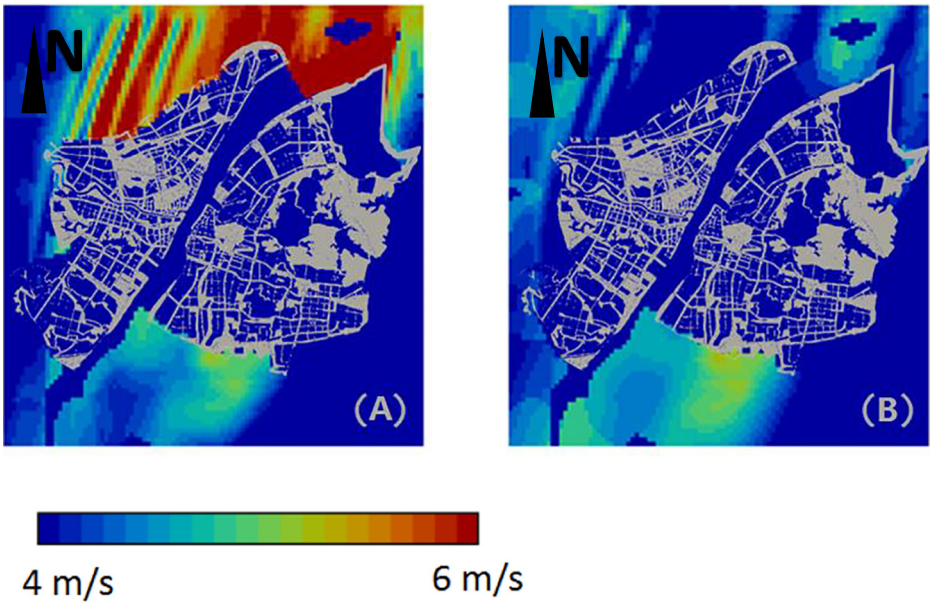

Fig. 12. Map of distribution of wind speed in Case_high-density (A) and Case_high-rise (B) at 20:00.

rise could be higher, which can greatly increase the evaporation and remove heat from the urban canopy. In contrast, the air temperature before dawn in Case_high-density is lower than that in Case_high-rise. We assumed that this was due to the effect of air flow obstruction by high buildings. To confirm our hypothesis, we compared the wind speed of these two cases along the wind direction and show the results in Fig. 9.

Fig. 9 presents the wind speed for the two cases along the A–A' axis shown in Fig. 8, where the axis is parallel to the northeast wind direction. As expected, due to the air flow obstruction effect, the wind speed in Case_high-rise gradually decreases along the axis from the rural to urban center. However, in the same local wind field, the wind speed in Case_high-density does not decrease, and, to the contrary, due to the air buoyancy caused by heat from the urban center, the wind speed increases slightly along the axis.

In comparing the cases, we discovered that the UHI phenomenon in Case_high_density is more significant during the day time, whereas due to the air flow obstruction effect of high buildings, the UHI phenomenon in Case_high_building is more significant during the night. The impacts of the two different patterns of compact city development (represented by the two cases) on the critical values of wind speed, which could mitigate the UHI phenomenon, are also different.

Fig. 10 presents a scatter plot of UHI intensity and wind speed for the Qingshan sampling zone, where black circles represent Case_high-rise, and red triangles represent Case_high-density. Clearly, UHI intensity and wind speed are both quite high in Case_high-density, while both factors are lower in Case_high-rise. Moreover, the critical value of wind speed to mitigate the UHI phenomenon is lower in Case_high-rise.

When the UHI intensity (y-axis) equals zero, the critical values of wind speed in Case_high-rise are 7.1 m/s and 10.7 m/s at 12:00 and 17:00, respectively. Similarly, the critical values of wind speed in Case_high-density are 7.7 m/s and 16.9 m/s at 12:00 and 17:00, respectively. Thus, Case_high-rise exhibits a higher potential to mitigate the UHI phenomenon than does Case_high-density.

6. Discussion

According to the NBS of China annual report, by the end of 2014, 54.7% of the total population will live in urban areas. Cities not only keep expanding, but they also become progressively more compact. Due to the rapid urbanization, great swathes of green space and lake area have been transformed into urban land. The decreases in lake area have caused the increase in UHI intensity, while simultaneously increasing the critical value of wind speed which could mitigate the UHI phenomenon. On comparing the two development patterns for compact cities, we discovered that when cities become progressively higher, air temperature at day time is lower than in the high-density development pattern, due to the shading effect of high buildings. However, during night time, air temperature is higher in the high-rise case due to the air flow obstruction effect of high buildings. Through analysis of the critical values of wind speed needed to mitigate the UHI phenomenon, we discovered that the high-density development pattern requires higher wind speed to mitigate the UHI phenomenon. Although the critical value of wind speed in the high-rise case is relatively low, we still doubt whether the wind speed in the high-rise case can reach the needed value, due to the air flow obstruction effect of the high buildings.

In addition to the above results, we also discuss the impact of urban morphology changes on the micro-climate of the downwind rural area. As discussed in many studies, the micro-climate of the downwind rural area is greatly affected by its upwind urban area. Oke et al. demonstrated that the range of urban impact on rural areas may reach 30 km, and the broadest range is almost 100 km.

As shown in Figs. 11 and 12, the impact of the two development patterns of compact cities on the air temperature and wind speed of the downwind rural area are quite different. At 20:00, the air temperature of the downwind rural area in the high-density case is approximately 34 °C (Fig. 10A), while the air temperature in the high-rise case is lower than 33.5 °C (Fig. 10B). The higher air temperature of the downwind rural area in the high-density case is due to the higher wind speed. As a result, the heat gained in the urban center is "blown" towards the downwind rural area, causing its air temperature to rise. Under the same local wind field, the wind speed of the downwind rural area in the high-rise case is only 70% of the high-density case, and demonstrates that the air flow obstruction effect of high buildings can extend as far as the downwind rural area.

7. Conclusions

With rapid urbanization, the land-use and urban morphology of cities in China have changed substantially in recent years. This study investigated the impact of decreasing lake area and changing urban morphology on the UHI phenomenon and selected Wuhan City as an example. Next, we arrived at the following conclusions.

1. When the lake area decreased by 130 km^2 in the built-up area of Wuhan, UHI intensity increased by 0.2° C-0.4° C.
2. When the lake area decreased by 130 km^2 in the built-up area of Wuhan, the critical value of wind speed needed to mitigate the UHI phenomenon increased and even doubled at 04:00.
3. To fulfil the requirements of urban development by 2020, we assumed that Wuhan will become progressively more compact with higher density. In this case, the UHI phenomenon becomes progressively more serious, and the critical value of wind speed needed to mitigate the UHI phenomenon increases significantly.
4. Although UHI intensity did not increase notably in the high-rise case, wind speed decreased substantially. Moreover, despite this finding, the critical value of wind speed needed to mitigate the UHI phenomenon was not high. Thus, due to the low wind speed caused by the wind flow obstruction effect of high buildings, the capacity of mitigating the UHI phenomenon in the high-rise case was shown to be unfavorable,.
5. In comparison, we discovered that air temperature differences between these two development patterns can reach 1° C and that at 12:00 and 17:00, respectively, the critical values of wind speed in the high-density case were 1.5 and 2 times higher than those of the high-rise case.
6. The impacts of the two development patterns of compact cities on the air temperature and wind speed in the downwind rural areas were quite different. The air temperature of the downwind area in the high-density case was 0.5°C higher than that of the high-rise case, however, wind speed of high-rise case was 70% of high-density case. Additionally, the critical values of wind speed needed to mitigate the UHI phenomenon in the high-density case was 2 m/s higher than that of the high-rise case.

In this study we applied the WRF/UCM as simulation tool, which is a professional meteorological software for urban climate study, however, with simple and rough urban model. This more or less will have an impact on the accuracy of the results. Therefore, we are still searching for a method of connecting WRF/UCM with Computational Fluid Dynamic (CFD) technique to improve the accuracy of the future works.

Acknowledgements

This work was supported by the State Key Program of National Natural Science of China (Grant No. 51538004), the National Natural Science Fund Youth Project (Grant No. 51708237), the 57th China Postdoctoral Science Foundation Funded Project (Grant No. 2015M572144), the Independent Innovation Fund of Huazhong University of Science and Technology (Grant No. 0118220100), and the JURC Short-Term Internship Program (Grant No. 2016-03).

Conflict of interest

The authors have no conflicts of interest to declare.

Role of the funding source

None.

References

Alcazar, S.S., Olivieri, F., Neila, J., 2016. Green roofs: experimental and analytical study of its potential for urban microclimate regulation in Mediterranean–continental climates. Urban Clim. 17, 304–317.

Avolio, E., Federico, S., Miglietta, M.M., Lo Feudo, T., Calidonna, C.R., Sempreviva, A.M., 2017. Sensitivity analysis of WRF model PBL schemes in simulating boundary-layer variables in southern Italy: an experimental campaign. Atmos. Res. 192, 58–71.

Birch, L., Cronin, T., Tziperman, E., 2017. Glacial inception on Baffin Island: the role of insolation, meteorology, and topography. J. Clim. 30, 4047–4064.

CBN Weekly, 2015. China City Commercial Appeal List 2016 8 May.

Chen, F., Dudhia, J., 2001. Coupling an advanced land surface–hydrology model with the Penn state–NCAR MM5 modeling system. Part I: model implementation and sensitivity. Mon. Weather Rev. 129, 569–585.

Chen, F., Kusaka, H., Bornstein, R., Ching, J., Grimmond, C.S.B., Grossman-Clarke, S., Loridan, T., Manning, K.W., Martilli, A., Miao, S., Sailor, D., Salamanca, F.P., Taha, H., Tewari, M., Wang, X., Wyszogrodzki, A.A., Zhang, C., 2011. The integrated WRF/urban modelling system: development, evaluation, and applications to urban environmental problems. Int. J. Climatol. 31, 273–288.

Dhar, T.K., Khirfan, L., 2017. A multi-scale and multi-dimensional framework for enhancing the resilience of urban form to climate change. Urban Clim. 19, 72–91.

Fahmy, M., Sharples, S., 2009. On the development of an urban passive thermal comfort system in Cairo, Egypt. Build. Environ. 44, 1907–1916.

Feyisa, G.L., Meilby, H., Jenerette, G.D., Pauliet, S., 2016. Locally optimized separability enhancement indices for urban land cover mapping: exploring thermal environmental consequences of rapid urbanization in Addis Ababa, Ethiopia. Remote Sens. Environ. 175, 14–31.

Fu, P., Weng, Q., 2016. A time series analysis of urbanization induced land use and land cover change and its impact on land surface temperature with Landsat imagery. Remote Sens. Environ. 175, 205–214.

Gaur, A., Eichenbaum, M.K., Simonovic, S.P., 2018. Analysis and modelling of surface urban Heat Island in 20 Canadian cities under climate and land-cover change. J. Environ. Manag. 206, 145–157.

Hsieh, C.-M., Aramaki, T., Hanaki, K., 2011. Managing heat rejected from air conditioning systems to save energy and improve the microclimates of residential buildings. Comput. Environ. Urban. Syst. 35, 358–367.

Kusaka, H., Kondo, H., Kikegawa, Y., Kimura, F., 2001. A simple single-layer urban canopy model for atmospheric models: comparison with multi-layer and slab models. Bound.-Layer Meteorol. 101, 329–358.

Li, X., Zhou, Y., Asrar, G.R., Imhoff, M., Li, X., 2017. The surface urban heat island response to urban expansion: a panel analysis for the conterminous United States. Sci. Total Environ. 605-606, 426–435.

Lin, P., Lau, S.S.Y., Qin, H., Gou, Z., 2017. Effects of urban planning indicators on urban heat island: a case study of pocket parks in high-rise high-density environment. Landsc. Urban Plan. 168, 48–60.

Lin, B.B., Egerer, M.H., Liere, H., Jha, S., Bichier, P., Philpott, S.M., 2018. Local- and landscape-scale land cover affects microclimate and water use in urban gardens. Sci. Total Environ. 610-611, 570–575.

Liu, X., Tian, G., Feng, J., Wang, J., Kong, L., 2018. Assessing summertime urban warming and the cooling efficacy of adaptation strategy in the Chengdu-Chongqing metropolitan region of China. Sci. Total Environ. 610-611, 1092–1102.

Lopes, A., Saraiva, J., Alcoforado, M.J., 2011. Urban boundary layer wind speed reduction in summer due to urban growth and environmental consequences in Lisbon. Environ. Model. Softw. 26, 241–243.

Mlawer, E.J., Taubman, S.J., Brown, P.D., Iacono, M.J., Clough, S.A., 1997. Radiative transfer for inhomogeneous atmospheres: RRTM, a validated correlated-k model for the longwave. J. Geophys. Res. Atmos. 102, 16663–16682.

Monin, A., Obukhov, A., 1954. Basic laws of turbulent mixing in the surface layer of the atmosphere. Contrib. Geophys. Inst. Acad. Sci. 24, 163–187.

Morris, K.I., Chan, A., Salleh, S.A., Ooi, M.C.G., Oozeer, M.Y., Abakr, Y.A., 2016. Numerical study on the urbanisation of Putrajaya and its interaction with the local climate, over a decade. Urban Clim. 16, 1–24.

Niu, W.Y., 2013. China New Urbanization Report. Science Press, Beijing.

Nunez, M., Oke, T.R., 1977. The energy balance of an urban canyon. J. Appl. Meteorol. 16, 11–19.

dos Santos, A.R., de Oliveira, F.S., da Silva, A.G., Gleriani, J.M., Gonçalves, W., Moreira, G.L., Silva, F.G., Branco, E.R.F., Moura, M.M., da Silva, R.G., Juvanhol, R.S., de Souza, K.B., Ribeiro, C.A.A.S., de Queiroz, V.T., Costa, A.V., Lorenzon, A.S., Domingues, G.F., Marcatti, G.E., de Castro, N.L.M., Resende, R.T., Gonzales, D.E., Telles, L.A.A., Teixeira, T.R., dos Santos, G.M.A.D.A., Mota, P.H.S., 2017. Spatial and temporal distribution of urban heat islands. Sci. Total Environ. 605-606, 946–956.

Sato, T., Murakami, S., Ooka, R., Yoshida, S., 2008. Analysis of regional characteristics of the atmospheric heat balance in the Tokyo metropolitan area in summer. J. Wind Eng. Ind. Aerodyn. 96, 1640–1654.

Sharma, R., Joshi, P.K., 2016. Mapping environmental impacts of rapid urbanization in the National Capital Region of India using remote sensing inputs. Urban Clim. 15, 70–82.

Suckall, N., Fraser, E., Forster, P., Mkwambisi, D., 2015. Using a migration systems approach to understand the link between climate change and urbanisation in Malawi. Appl. Geogr. 63, 244–252.

The Economist, 2012. Urban Life: Open-air Computers 27 October.

Thompson, G., Rasmussen, R.M., Manning, K., 2004. Explicit forecasts of winter precipitation using an improved bulk microphysics scheme. Part I: description and sensitivity analysis. Mon. Weather Rev. 132, 519–542.

Tsunematsu, N., Yokoyama, H., Honjo, T., Ichihashi, A., Ando, H., Shigyo, N., 2016. Relationship between land use variations and spatiotemporal changes in amounts of thermal infrared energy emitted from urban surfaces in downtown Tokyo on hot summer days. Urban Clim. 17, 67–79.

Vox, G., Blanco, I., Fuina, S., Campiotti, C.A., Mugnozza, G.S., Schettini, E., 2017. Evaluation of wall surface temperatures in green facades. Proc. Inst. Civil Eng-Eng. Sustain. 170, 334–344.

Wai, K.M., Wang, X.M., Lin, T.H., Wong, M.S., Zeng, S.K., He, N., Ng, E., Lau, K., Wang, D.H., 2017. Observational evidence of a long-term increase in precipitation due to urbanization effects and its implications for sustainable urban living. Sci. Total Environ. 599-600, 647–654.

Wu, H., Ye, L.-P., Shi, W.-Z., Clarke, K.C., 2014. Assessing the effects of land use spatial structure on urban heat islands using HJ-1B remote sensing imagery in Wuhan, China. Int. J. Appl. Earth Obs. Geoinf. 32, 67–78.

Xue, L., Edwards, R., Huggins, A., Lou, X., Rasmussen, R., Tessendorf, S., Holbrook, P., Blestrud, D., Kunkel, M., Glenn, B., Parkinson, S., 2017. WRF large-eddy simulations of chemical tracer deposition and seeding effect over complex terrain from ground- and aircraft-based *AgI* generators. Atmos. Res. 190, 89–103.

Yan, H., Wu, F., Dong, L., 2018. Influence of a large urban park on the local urban thermal environment. Sci. Total Environ. 622-623, 882–891.

Yao, R., Wang, L., Huang, X., Niu, Z., Liu, F., Wang, Q., 2017. Temporal trends of surface urban heat islands and associated determinants in major Chinese cities. Sci. Total Environ. 609, 742–754.

Zhou, X., Ooka, R., Chen, H., Kawamoto, Y., Kikumoto, H., 2016. Impacts of inland water area changes on the local climate of Wuhan, China. Indoor Built Environ. 25, 296–313.